Revista de Chimie
https://revistadechimie.ro
https://doi.org/10.37358/Rev.Chim.1949

The Mechanism of Selective Separation of Antimony from Chloride Leachate of Copper Anode Slime

YANLIANG ZENG, CHUNFA LIAO*, ZHENGXIN XU, FUPENG LIU
Faculty of Metallurgy and Chemical Engineering, Jiangxi University of Science and Technology, Ganzhou 341000, China

Abstract: *The mechanism of selective separation of antimony from copper anode slime leachate is studied. Density functional theory is used to calculate the unit cell energy, band structure, density of states, number of charge distributions and overlap populations of the* $SbCl_3$ *hydrolysates SbOCl,* Sb_3O_4Cl *and* $Sb_4O_5Cl_2$*, and these are studied by infrared spectroscopy. The pathways for formation of SbOCl,* Sb_3O_4Cl *and* $Sb_4O_5Cl_2$ *in water, ethanol and ethylene glycol systems are clarified. The results show that the energy of the SbOCl unit cell is the lowest, and the structure is more stable. SbOCl exhibits strong electronic localization, weak orbital expansion, and more stability; SbOCl has a wider pseudoenergy gap, and its covalent bonds are stronger than those of* Sb_3O_4Cl *and* $Sb_4O_5Cl_2$*. Hydrolysis of* $SbCl_3$ *leads to preferential generation of more stable structures. The charge distribution, the sizes of overlap populations, and the infrared spectra indicate that* $SbCl_3$ *has been hydrolysed. There are two basic paths for the process of alcoholysis: a water- or alcohol-ionized hydroxyl replaces one chlorine atom in* $SbCl_3$ *to form an* $[Sb(OH)Cl_2]$ *monomer, and as the degree of hydrolysis increases, the H and Cl atoms are removed to form SbOCl. Conversely,* Sb_3O_4Cl*,* $Sb_4O_5Cl_2$ *or Sb atoms may be formed an [Sb-OH] monomer generated directly by water- or alcohol-ionised hydroxyl groups, and Cl atoms replace the H atom in the hydroxyl group of the [Sb-OH] monomer to form SbOCl,* Sb_3O_4Cl *and* $Sb_4O_5Cl_2$*.*

Keywords: *copper anode slime, antimony, density functional method, hydrolysis mechanism, infrared spectrum*

1. Introduction

Copper anode slime is an important by product of the copper electrolytic refining process, and its yield accounts for approximately 0.2%-0.8% of the output of refined copper [1]. In 2019, China's copper anode slime output reached 78,000 t. Copper anode slime is rich in many rare and precious metals, such as gold, silver, selenium, tellurium, antimony, bismuth, and metals of the platinum group [1,2]. At present, there are many processes for treating copper anode slime to recover these valuable metals, such as the traditional pyrometallurgical process [3-5], a combined process of beneficiation and metallurgy [3,5,6], the Kaldor furnace process [3,5], and a hydrometallurgical process [3,5,7]. Nevertheless, many problems still arise in these processes during industrial production, such as high energy consumption for pyrometallurgical processes, heavy pollution for combined processes, poor raw material applicability for Kaldor furnace processes, and difficult subsequent metal separation for hydrometallurgical processes. To recover valuable metals from anode slime in a more economical, efficient and environmentally-sound fashion, an innovative process was proposed and industrialized at Jiangxi Copper Co., Ltd. The process mainly includes "mixed acid leaching of bismuth and antimony – separation of Cu by sulfated roasting followed by water leaching - sodium hydroxide leaching of tellurium – recovery and separation of gold and silver". In this process the following metals in the indicated proportions are effectively separated from copper anode slime: > 9-% Bi, 95% Sb, 90% Se, 95% Cu, 95% Au and 96% Ag. This shows that the process allows comprehensive recovery of valuable metals from copper anode slime. However, there are few reports on the mechanism of selective separation of valuable metals from copper anode slime. This makes it difficult to accurately control the metal separation process, which is not conducive to the stable operation of smelters.

**email:liaochfa@163.com*

In this proposed process, antimony is leached into solution by leaching with a mixed acid (sulfuric acid and hydrochloric acid). Then, antimony is hydrolysed to its oxychlorides by adjusting the *p*H of the leachate to achieve selective separation from other metal elements [8-10]. Although the separation of antimony can be carried out effectively at this stage, the hydrolysis mechanism of antimony needs further clarification.

The valence states of antimony are mainly +5 and +3. Zheng et al. [11,12] studied the hydrolysis process of Sb^{5+} and clarified that the initial hydrolysis product of Sb^{5+} was primarily amorphous antimony oxide, but with decreases of acidity and ageing time the hydrolysate changes from amorphous to crystalline. Tian et al. [13-19] carried out the hydrolysis of Sb^{3+} in a chloride salt system to probe aspects of the hydrolysis process such as equilibrium state, thermodynamics, kinetics, and hydrolysis products. The study clarified the mechanism for Sb^{3+} hydrolysis. Due to the difference in reaction conditions, operating methods, environmental conditions and other factors, the hydrolysis products of Sb^{3+} and Sb^{5+} were more complicated, and the amorphous and crystalline products were mixed. Therefore, the antimony hydrolysis process and mechanism were unclear and controversial, and the microstructure was not analysed.

Based on first principles and density functional theory, the reaction pathway of the hydrolysis process was studied by calculating the electronic structure, unit cell structure, energy band structure, density of states, charge layout number and overlapping population for $SbCl_3$, SbOCl, Sb_3O_4Cl and $Sb_4O_5Cl_2$. Moreover, the oxidation state changes occurring during hydrolysis were further verified by infrared spectroscopy analysis.

2. Materials and methods

Using first-principles density functional theory (DFT) combined with the plane pseudopotential method, the CASTEP [20,21] module of MS software was used to optimize the unit cell structure and calculate the unit cell system energy and band structure of antimony compounds, as well as the total density of states and sub-state density, number of charge layouts, and number of overlapping clusters. The method established unit cell models for $SbCl_3$, SbOCl, Sb_3O_4Cl, and $Sb_4O_5Cl_2$ according to the relevant parameters in Table 1; the generalized gradient approximation (GGA) was used to correct the exchange effect from interactions between electrons in different unit cells; The Perdew-Burke-Ernzerh (PBE) in Generalized Gradient Approximation (GGA) was used to deal with interactions between electrons. The Monkhorst-Pack scheme was used to select the grid points in k-space and calculate the total energy and charge density of the system in the Brillouin zone. Brillouin zone k vectors were selected as 1×2×2, 2×2×3, 2×4×3 and 3×4×1; plane wave truncation energies were set to 244.9 eV, 489.8 eV, 489.8 eV and 489.8 eV, the self-consistent accuracy was set to 2.0×10-6 eV/atom, and the force acting on each atom did not exceed 0.05 eV/nm.

Table 1. Unit cell parameters

Title	Space group name	Lattice parameters					
		a	b	c	α	β	γ
$SbCl_3$	P n m a	8.11100Å	9.41900Å	6.31300Å	90.0000°	90.0000°	90.0000°
SbOCl	P 21/a	9.54000Å	10.77000Å	7.94000Å	90.0000°	90.0000°	90.0000°
Sb_3O_4Cl	P 2/c	9.65310Å	5.30590Å	5.59810Å	90.0000°	94.7450°	90.0000°
$Sb_4O_5Cl_2$	P 21/c	6.23800Å	5.11120Å	13.53800Å	90.0000°	97.2170°	90.0000°

Solid $SbCl_3$ and a certain concentration of $SbCl_3$ solution were used to carry out hydrolysis and alcoholysis reactions in different systems. $SbCl_3$ solid powder was dissolved in hydrochloric acid to prepare a solution with concentrations of 0.05 mol/L Sb^{3+} and 1 mol/L Cl^-, and this was added to equal volumes of deionized water, ethanol, and ethylene glycol. The reactions were stirred at room temperature (25℃) for 2 h, the *p*H values of the solutions were adjusted to 2 with aqueous ammonia, they were placed in an ultrasonic reactor for 1 h, and the dry product was obtained by centrifugal filtration at 60℃ for 6h.

The filtrate was analysed by fourier infrared spectroscopy (FTIR-650, Tianjin Gangdong Technology Co., Ltd.).

3. Results and discussions

3.1. First principles studies

3.1.1. Energy analysis

The lower the total energy of the unit cell is, the more stable the structure of the unit cell [22-24]. The optimized structures and energies of $SbCl_3$, SbOCl, Sb_3O_4Cl and $Sb_4O_5Cl_2$ were calculated, and the unit cell energy of each substance is shown in Table 2.

Table 2. Unit cell energy of each substance.

Physical phase	Energy
$SbCl_3$	-14616.055 eV
SbOCl	-38974.208 eV
Sb_3O_4Cl	-18672.508 eV
$Sb_4O_5Cl_2$	-25168.427 eV

It can be seen from Table 2 that the SbOCl unit cell has the lowest energy. A preliminary analysis of the hydrolysis of $SbCl_3$ suggests that priority will be given to the generation of SbOCl, due to its low energy and stable structure.

3.1.2. Energy band analysis

The wider the energy band is, the greater the fluctuations, indicating that the effective mass of the electrons in the energy band is smaller, the extent of delocalization is greater, and the atomic orbitals that make up this energy band are more extended and more accessible for reactions. A narrow energy band width indicates that the eigenstate of the energy band is mainly composed of atomic orbitals at a certain lattice point in the local area. The electrons in this energy band are strongly localized, exhibiting limited orbital expansion and contributing to greater stability [25, 26].

The calculated energy band diagram for each substance is shown in Figure 1. This shows that the energy band of $SbCl_3$ extends from -28.5 eV to 15.9 eV, so the bandwidth is 44.4 eV and the band gap is 4.152 eV; the energy band of SbOCl extends from -28.6 eV to 16.4 eV, so the bandwidth is 45.0 eV and the band gap width is 3.101 eV; the energy band of Sb_3O_4Cl extends from -28.6 eV to 17.8 eV, so the bandwidth is 46.4 eV and the band gap is 2.737 eV; the energy band of $Sb_4O_5Cl_2$ extends from -28.8 eV to 17.1 eV, so the bandwidth is 45.9 eV and the band gap is 2.730 eV. By comparison, it can be seen that SbOCl has the narrowest energy band width and smallest fluctuations, indicating that electronic localization in the SbOCl energy band is very strong, orbital expansion is limited, the properties are relatively stable, the energy of the unit cell is consistent, and SbOCl more easily forms a stable structure.

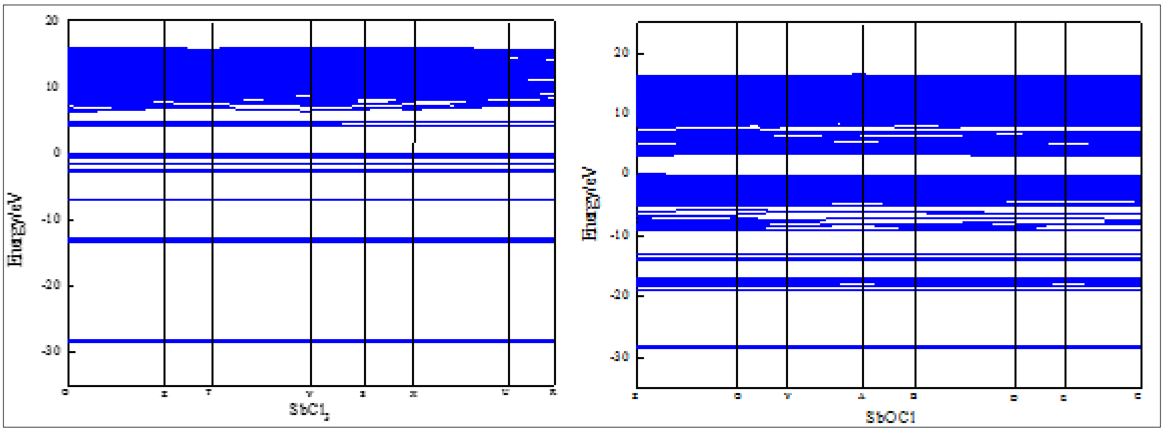

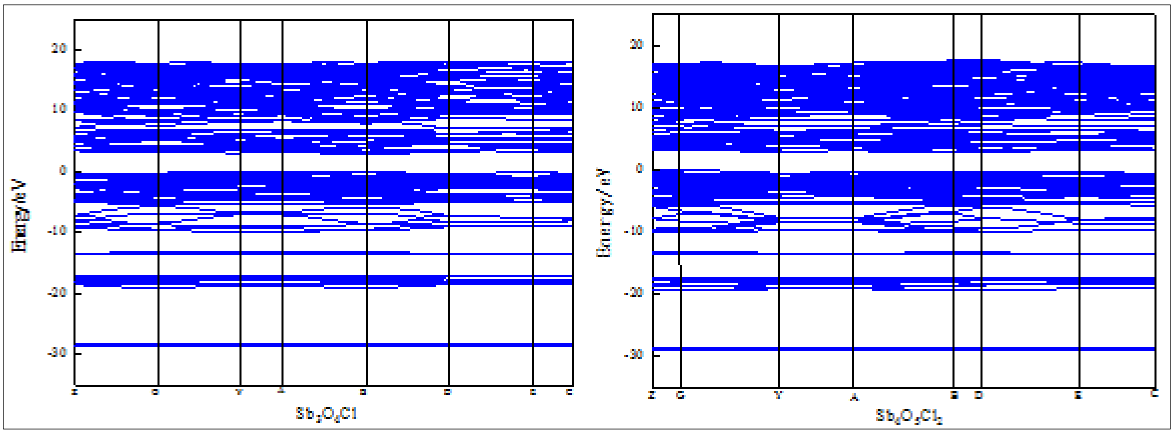

Figure 1. Energy bands of $SbCl_3$, SbOCl, Sb_3O_4Cl and $Sb_4O_5Cl_2$

3.1.3. Density analysis

The size of the pseudoenergy gap in the density of states map (the peaks and valleys of the low-energy bonding state and the high-energy antibonding region produce the pseudoenergy gap) reflects the strength of covalent bonding. The wider the pseudoenergy gap is, the greater the covalent character. The larger the abscissa of the peak density of states, the easier it is for extranuclear electrons to be distributed in the high-energy region, and the easier it is to remove electrons. In contrast, it is also easier to accept electrons [27, 28].

The calculated density of states diagram for each substance is shown in Figure 2. It can be seen that the pseudo-energy gap of $SbCl_3$ extends from -0.386 to 4.290 eV and the pseudo-energy gap is 4.676 eV, which is mainly contributed by the electrons in Cl 2p and Sb 6s and 6p orbitals; the pseudo-energy gap of SbOCl extends from -1.400 to 3.930 eV and the pseudo-energy gap is 5.330 eV; the pseudo-energy gap of Sb_3O_4Cl extends from -0.393 to 3.610 eV and the pseudo-energy gap is 4.003 eV; and the pseudo-energy gap of $Sb_4O_5Cl_2$ extends from -0.524 to 3.500 eV and the pseudo-energy gap is 4.024 eV. Antimony oxychlorides are mainly contributed by electrons on the electron orbitals of Cl2p, O2p and Sb6s6p. By comparison, it can be seen that the pseudoenergy gap of SbOCl is the largest, and the extent of covalent bonding among its atoms is the greatest. Therefore, the hydrolysis of $SbCl_3$ more easily generates stable SbOCl.

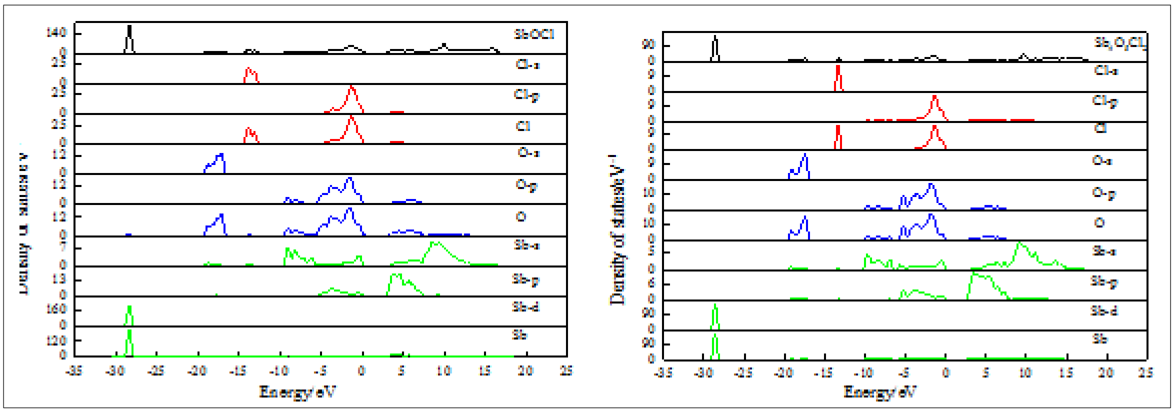

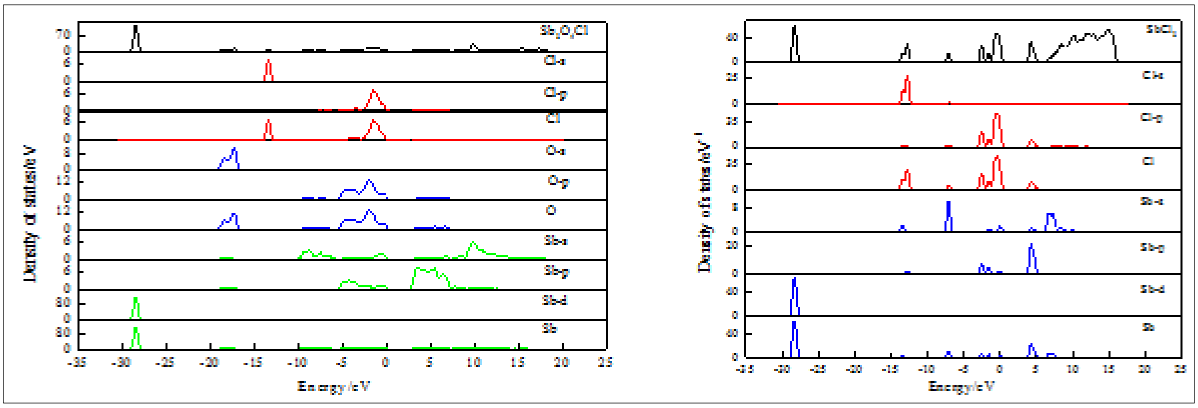

Figure 2. The state density and fractional state density of $SbCl_3$, SbOCl, Sb_3O_4Cl, and $Sb_4O_5Cl_2$

3.1.4. The charge distribution number analysis

The charge distribution number can reflect the gain or loss of electrons in an atom. A positive charge indicates a loss of electrons, and a negative charge indicates a gain of electrons. The gain and loss of electrons can strengthen the bonding interactions between atoms. The greater the number of electrons transferred, the stronger the bond interaction between atoms, and vice versa [29].

The calculated formal charge for each substance is shown in Table 3. It can be seen from Table 3 that the $SbCl_3$ unit cell contains 12 Cl atoms, and each Cl atoms contains 0.39 extra electrons; there are 4 Sb atoms and each Sb atom has lost 1.17 electrons; Since all Sb atoms combined have lost 4.68 electrons, this matches the 0.39 electrons lost by each Cl atom.

From the formal charges of SbOCl, it can be concluded that each of the 12 Sb atoms has lost either 1.57, 1.39, or 1.37 electrons; the 12 O atoms have all gained 0.97 electrons; there are 12 Cl atoms and groups of 4 Cl atoms each have received 0.43, 0.42, or 0.57 electrons. The greater the number of electrons transferred, the stronger the ionic bonding between atoms. Since oxygen atoms have gained more electrons than chlorine atoms, the [Sb-O] ionic bond is stronger than the [Sb-Cl] ionic bond. Based on this analysis, SbOCl can lose Cl atoms in the preparation of Sb_2O_3.

The formal charges of Sb_3O_4Cl show that among the 8 O atoms, 4 receive 0.98 and 4 receive 0.97 electrons; the number of excess electrons in both Cl atoms is 0.56; the number of electrons lost by the 6 Sb atoms includes 4 atoms with a deficiency of 1.45 electrons and 2 atoms with a deficiency of 1.56 electrons. The Sb atoms that lose 1.45 electrons exist in the [SbO_2-O-SbO_2] unit; that is, the 2 Sb atoms that lose 1.45 have lost a total of 2.9 electrons, and 2 O atoms have received 0.97 electrons, and 1 O atom received 0.98 electrons. The Sb atom that lost 1.56 electrons is bound to 1 Cl atom with an excess of 0.56 electrons and 1 O atom with an excess of 0.98 electrons. That is, the Sb-O ionic bond within [SbO_2] units in [SbO_2-O-SbO_2] (or [Sb_2O_3]) is stronger than the bonds to the bridging O atom shared by two [SbO_2] units in [SbO_2-O-SbO_2]. Another antimony atom exists in the form of [SbOCl], where the Sb-O bond is stronger than the Sb-Cl bond.

From the formal charges of $Sb_4O_5Cl_2$, it can be concluded that of the 10 O atoms there are 4 O atoms receiving 0.99 electrons, 4 O atoms receiving 0.96 electrons and 2 O atoms receiving 1.03 electrons; the number of electrons in 4 Cl atoms is 0.57; the numbers of electrons lost by the 8 Sb atoms include 1.51 (4 atoms) and 1.53 (4 atoms). An Sb atom that lost 1.45 electrons exists in the [SbO_2Cl-O-SbO_2Cl] unit; i.e., the 4 Sb atoms that lost 1.51 elections provide a total loss of 6.04 electrons; 3 O atoms each receive 0.96 electrons, 1 O atom receives 0.99 electrons, 1 O atom receives 1.03 electrons and 2 Cl atoms each receive 0.57 electrons; 4 Sb atoms each lose 1.53 electrons, for a total of 6.12 lost electrons; 1 O atom receives 0.96 electrons, 3 O atoms each receive 0.99 electrons, 1 O atom receives 1.03 electrons and 2 Cl atoms each receive 0.57 electrons. That is, the Sb-O ionic bond within [Sb_2O_2Cl] units in [Sb_2O_2Cl-O-Sb_2O_2Cl] (or [Sb_4O_5Cl]) is stronger than that in the O atom shared by two [Sb_2O_2Cl] units in [Sb_2O_2Cl-O-Sb_2O_2Cl].

Table 3. Formal charge numbers

Unit cell	Species	Ion	s	p	d	f	Total	Charge(e)
$SbCl_3$	Cl	1	1.97	5.41	0.00	0.00	7.39	-0.39
	Cl	2	1.97	5.41	0.00	0.00	7.39	-0.39
	Cl	3	1.97	5.41	0.00	0.00	7.39	-0.39
	Cl	4	1.97	5.41	0.00	0.00	7.39	-0.39
	Cl	5	1.97	5.41	0.00	0.00	7.39	-0.39
	Cl	6	1.97	5.41	0.00	0.00	7.39	-0.39
	Cl	7	1.97	5.41	0.00	0.00	7.39	-0.39
	Cl	8	1.97	5.41	0.00	0.00	7.39	-0.39
	Cl	9	1.97	5.42	0.00	0.00	7.39	-0.39
	Cl	10	1.97	5.42	0.00	0.00	7.39	-0.39
	Cl	11	1.97	5.42	0.00	0.00	7.39	-0.39
	Cl	12	1.97	5.42	0.00	0.00	7.39	-0.39
	Sb	1	1.91	1.92	10.00	0.00	13.83	1.17
	Sb	2	1.91	1.92	10.00	0.00	13.83	1.17
	Sb	3	1.91	1.92	10.00	0.00	13.83	1.17
	Sb	4	1.91	1.92	10.00	0.00	13.83	1.17
SbOCl	O	1	1.90	5.07	0.00	0.00	6.97	-0.97
	O	2	1.90	5.07	0.00	0.00	6.97	-0.97
	O	3	1.90	5.07	0.00	0.00	6.97	-0.97
	O	4	1.90	5.07	0.00	0.00	6.97	-0.97
	O	5	1.90	5.07	0.00	0.00	6.97	-0.97
	O	6	1.90	5.07	0.00	0.00	6.97	-0.97
	O	7	1.90	5.07	0.00	0.00	6.97	-0.97
	O	8	1.90	5.07	0.00	0.00	6.97	-0.97
	O	9	1.90	5.07	0.00	0.00	6.97	-0.97
	O	10	1.90	5.07	0.00	0.00	6.97	-0.97
	O	11	1.90	5.07	0.00	0.00	6.97	-0.97
	O	12	1.90	5.07	0.00	0.00	6.97	-0.97
	Cl	1	1.97	5.46	0.00	0.00	7.43	-0.43
	Cl	2	1.97	5.46	0.00	0.00	7.42	-0.42
	Cl	3	1.97	5.60	0.00	0.00	7.57	-0.57
	Cl	4	1.97	5.46	0.00	0.00	7.43	-0.43
	Cl	5	1.97	5.46	0.00	0.00	7.42	-0.42
	Cl	6	1.97	5.60	0.00	0.00	7.57	-0.57
	Cl	7	1.97	5.46	0.00	0.00	7.43	-0.43
SbOCl	Cl	8	1.97	5.46	0.00	0.00	7.42	-0.42
	Cl	9	1.97	5.60	0.00	0.00	7.57	-0.57
	Cl	10	1.97	5.46	0.00	0.00	7.43	-0.43
	Cl	11	1.97	5.46	0.00	0.00	7.42	-0.42
	Cl	12	1.97	5.60	0.00	0.00	7.57	-0.57
	Sb	1	1.77	1.66	10.00	0.00	13.43	1.57
	Sb	2	1.83	1.77	10.00	0.00	13.61	1.39
	Sb	3	1.86	1.76	10.00	0.00	13.63	1.37
	Sb	4	1.77	1.66	10.00	0.00	13.43	1.57
	Sb	5	1.83	1.77	10.00	0.00	13.61	1.39
	Sb	6	1.86	1.76	10.00	0.00	13.63	1.37
	Sb	7	1.77	1.66	10.00	0.00	13.43	1.57
	Sb	8	1.83	1.77	10.00	0.00	13.61	1.39
	Sb	9	1.86	1.76	10.00	0.00	13.63	1.37
	Sb	10	1.77	1.66	10.00	0.00	13.43	1.57
	Sb	11	1.83	1.77	10.00	0.00	13.61	1.39
	Sb	12	1.86	1.76	10.00	0.00	13.63	1.37
Sb_3O_4Cl	O	1	1.90	5.07	0.00	0.00	6.97	-0.97
	O	2	1.90	5.08	0.00	0.00	6.98	-0.98
	O	3	1.90	5.07	0.00	0.00	6.97	-0.97
	O	4	1.90	5.08	0.00	0.00	6.98	-0.98
	O	5	1.90	5.07	0.00	0.00	6.97	-0.97
	O	6	1.90	5.08	0.00	0.00	6.98	-0.98
	O	7	1.90	5.07	0.00	0.00	6.97	-0.97
	O	8	1.90	5.08	0.00	0.00	6.98	-0.98
	Cl	1	1.96	5.60	0.00	0.00	7.56	-0.56
	Cl	2	1.96	5.60	0.00	0.00	7.56	-0.56

	Sb	1	1.82	1.73	10.00	0.00	13.55	1.45
	Sb	2	1.82	1.73	10.00	0.00	13.55	1.45
	Sb	3	1.82	1.73	10.00	0.00	13.55	1.45
	Sb	4	1.82	1.73	10.00	0.00	13.55	1.45
	Sb	5	1.80	1.63	10.00	0.00	13.44	1.56
	Sb	6	1.80	1.63	10.00	0.00	13.44	1.56
$Sb_4O_5Cl_2$	O	1	1.90	5.09	0.00	0.00	6.99	-0.99
	O	2	1.89	5.07	0.00	0.00	6.96	-0.96
	O	3	1.90	5.09	0.00	0.00	6.99	-0.99
	O	4	1.89	5.07	0.00	0.00	6.96	-0.96
	O	5	1.90	5.09	0.00	0.00	6.99	-0.99
	O	6	1.89	5.07	0.00	0.00	6.96	-0.96
	O	7	1.90	5.09	0.00	0.00	6.99	-0.99
	O	8	1.89	5.07	0.00	0.00	6.96	-0.96
	O	9	1.86	5.17	0.00	0.00	7.03	-1.03
$Sb_4O_5Cl_2$	O	10	1.86	5.17	0.00	0.00	7.03	-1.03
	Cl	1	1.97	5.60	0.00	0.00	7.57	-0.57
	Cl	2	1.97	5.60	0.00	0.00	7.57	-0.57
	Cl	3	1.97	5.60	0.00	0.00	7.57	-0.57
	Cl	4	1.97	5.60	0.00	0.00	7.57	-0.57
	Sb	1	1.81	1.66	10.00	0.00	13.47	1.53
	Sb	2	1.79	1.70	10.00	0.00	13.49	1.51
	Sb	3	1.81	1.66	10.00	0.00	13.47	1.53
	Sb	4	1.79	1.70	10.00	0.00	13.49	1.51
	Sb	5	1.81	1.66	10.00	0.00	13.47	1.53
	Sb	6	1.79	1.70	10.00	0.00	13.49	1.51
	Sb	7	1.81	1.66	10.00	0.00	13.47	1.53
	Sb	8	1.79	1.70	10.00	0.00	13.49	1.51

3.1.5. Overlap population analysis

The overlap population can be used to reflect the interaction between atoms, analyse the bonding properties between atoms and reflect the strength of bonds between atoms. The numbers for overlap populations are positive, which means that the atoms are bonded by covalent bonds. The larger the value is, the stronger the covalent bond and the more stable the unit cell structure; if the value for an overlap population is negative, it means that atoms are combined in the form of anti-bonds. The smaller the value, the stronger the repulsion between atoms and the weaker the stability; when the overlap population is 0, there are ionic bonds between atoms [30-32]. The calculated overlap populations for each substance are shown in Table 4.

Table 4. Overlap population

Unit cell	Bond	Population	Length(A)	Quantity	Unit cell	Bond	Population	Length(A)	Quantity
$SbCl_3$	Cl-Sb	0.29	2.40580	4	Sb_3O_4Cl	O-Sb	0.31	1.99466	4
	Cl-Sb	0.31	2.43414	8		O-Sb	0.32	2.00347	4
SbOCl	O-Sb	0.38	1.97743	4		O-Sb	0.27	2.06080	4
	O-Sb	0.36	1.99155	4		O-Sb	0.18	2.12257	4
	O-Sb	0.29	2.02392	4		O-Sb	0.06	2.29521	4
	O-Sb	0.23	2.05346	4		O-O	-0.06	2.69263	2
	O-Sb	0.22	2.08231	4		O-O	-0.06	2.74405	4
	O-Sb	0.21	2.09117	4		O-O	-0.08	2.90540	2
	O-Sb	0.07	2.25064	8		O-Sb	-0.05	2.98789	4
	Cl-Sb	0.34	2.41302	4	$Sb_4O_5Cl_2$	O-Sb	0.36	1.93722	4
	Cl-Sb	0.31	2.43370	4		O-Sb	0.37	1.98900	4
	O-O	-0.09	2.48546	2		O-Sb	0.23	2.05608	4
SbOCl	O-O	-0.09	2.54023	4		O-Sb	0.20	2.09237	4
	O-O	-0.05	2.75230	4		O-Sb	0.18	2.11698	4
	O-O	-0.03	2.95327	4		O-Sb	0.16	2.15594	4
	Cl-Sb	-0.05	2.90635	4		O-O	-0.09	2.51204	2
						O-O	0.00	2.56141	4
						O-O	-0.07	2.61251	4
						O-O	-0.08	2.88777	4
						Cl-Sb	0.13	2.93455	4

We can see that the overlap populations of $SbCl_3$ are both positive (0.29 and 0.31), indicating that Cl and Sb atoms are connected by covalent bonds. The sums of the overlapping populations of Sb-Cl bonds are 1.16 and 2.48, respectively and the total is 3.64; the greater the population, the stronger the stability of the covalent bond; therefore, each [$SbCl_3$] unit contains one Sb-Cl bond with an overlap population of 0.29 and two Sb-Cl bonds with overlap populations of 0.31. Therefore, since 0.31>0.29, when $SbCl_3$ is hydrolysed, the OH- produced by water ionization replaces a Cl atom from one of the Sb-Cl bonds with an overlap population of 0.29 and forms $Sb(OH)Cl_2$; subsequent loss of HCl leads to formation of SbOCl, Sb_3O_4Cl and $Sb_4O_5Cl_2$.

It can be seen from the list of SbOCl overlap populations that the overlap populations of Sb-O bonds are all positive, with values of 0.38, 0.36, 0.29, 0.23, 0.22, 0.21 and 0.07; this indicates that O and Sb atoms are connected by covalent bonds. The sums of the overlap populations of Sb-O bonds are 1.52, 1.44, 1.16, 0.92, 0.88, 0.84, and 0.56, and the total is 7.32. The overlap populations of O-O bonds are all negative, with values of -0.09, -0.05 and -0.03. This means that the O-O bond includes an antibonding contribution, i.e., the two O atoms repel each other. The more negative the value is, the stronger the repulsive force between atoms and the lower the stability of the unit cell; the sums of the O-O bond overlap populations are -0.54, -0.20 and -0.12, and the overall total is -0.86. Cl-Sb bonds exhibit both positive and negative overlaps, indicating that Cl-Sb bonds can include both covalent bonding and antibonding contributions. The positive overlap populations are 0.34 and 0.31, the sums of these positive overlap populations are 1.36 and 1.24, and the total is 2.60. The negative overlap populations of Cl-Sb bonds are -0.05, and the sum of the negative overlap populations is -0.20. It can be seen from the overlap populations of SbOCl that the stabilities of the SbOCl covalent bonds decrease in the order Sb-O > Sb-Cl (positive) > Sb-Cl (negative) > O-O.

From the overlap populations of Sb_3O_4Cl, we can see that the overlap populations of Sb-O bonds indicate the presence of covalent bonds and anti-bonds. The positive overlap populations of Sb-O bonds are 0.31, 0.32, 0.27, 0.18 and 0.06, and the sums of the positive Sb-O bond overlap populations are 1.24, 1.28, 1.08, 0.72, and 0.24, for a total of 4.56; another Sb-O bond shows a negative overlap population with a value -0.05, for a total of -0.20. Finally, the overlap populations of O-O bonds are -0.06 and -0.08. The sums of the O-O overlap populations are -0.36 and -0.16, and the total is -0.52, which means that the O-O bonds exhibit antibonding interactions; the 2 O atoms repel each other and the more negative value is, the stronger the repulsive force between atoms and the lower the stability of the unit cell. The overlap populations of Sb_3O_4Cl indicate that the stabilities of the covalent bonds in Sb_3O_4Cl decrease in the order Sb-O>Sb-O(Negative) > O-O.

The overlap populations of $Sb_4O_5Cl_2$ show that the overlap populations of the Sb-O bonds are all positive, with values of 0.36, 0.37, 0.23, 0.20, 0.18, and 0.16, which indicate that the O and Sb atoms are connected by covalent bonds. The sums of the overlap populations of Sb-O bonds are 1.44, 1.48, 0.92, 0.80, 0.72, and 0.64, and the total is 6.00. The overlap populations of O-O bonds are either negative or zero, indicating that both anti-bonds and ionic bonds are generated between O-O bonds. They can form ionic bonds, and the negative overlap populations for antibonding interactions are -0.09, -0.08 and -0.07, the sums of the overlap populations of O-O bonds are -0.18, -0.32 and -0.28, and the total is -0.78. The overlap populations of Cl-Sb bonds are all positive and exhibit values of 0.13, indicating that Cl and Sb are connected by a covalent bond; The total number of overlapping clusters of Sb-O bonds is 0.52. The overlap populations of $Sb_4O_5Cl_2$ show that the stabilities of $Sb_4O_5Cl_2$ covalent bond decrease in the order Sb-O > Sb-Cl > O-O (negative) > O-O (zero).

By comparing the overlap populations of SbOCl, Sb_3O_4Cl and $Sb_4O_5Cl_2$, it can be seen that the sum of the overlap populations in SbOCl covalent bonds is 9.92, the sum of the overlap populations for antibonding is -1.06, the sum of overlap populations for covalent bonds and overlap populations of antibonding orbitals for the aggregate population is 8.86; therefore, the covalent bonding effect is 9.36 times that of the anti-bonding effect. The greater the covalent bonding contribution is, the more stable the structure [33,34]; the sum of the aggregated overlap populations for Sb_3O_4Cl covalent bonds is 4.56, the sum of the overlap populations for antibonding interactions is -0.72, the overall sum of the overlap populations of both covalent bonding and antibonding is 3.84, so the covalent bonding effect is 6.33 times the effect of antibonding. For $Sb_4O_5Cl_2$, the sum of the overlap populations for covalent bonds is 6.52, the sum of the overlap populations for antibonding is -0.78, the overall sum is 5.74, and the effect of covalent bonding is greater than that of anti-bonding. The covalent bond of SbOCl is the strongest, the force between atoms is the largest, and the stability of the unit cell is the highest. Therefore, the $Sb(OH)Cl_2$ generated during the hydrolysis of $SbCl_3$ more easily continues on to eliminate HCl and generate SbOCl; that is, SbOCl is more stable than $Sb_4O_5Cl_2$ or Sb_3O_4Cl.

In summary, compared with Sb_3O_4Cl and $Sb_4O_5Cl_2$, SbOCl has the lowest unit cell energy, the narrowest energy bandwidth and the widest pseudoenergy gap, i.e., the strongest covalent bonds between Sb, O and Cl atoms. During the hydrolysis of $SbCl_3$, it is easier to generate stable SbOCl; from the formal charges, it can be seen that $SbCl_3$ preferentially breaks the [Sb-Cl] bond with the weaker bond energy and forms $Sb(OH)Cl_2$; among the group SbOCl, Sb_3O_4Cl and $Sb_4O_5Cl_2$, the [Sb-O] bond is stronger than the [Sb-Cl] bond, and it is easy to remove the Cl atom in a later stage of the process to obtain Sb_2O_3 or Sb powder. By comparing the overlap populations for antibonding interactions and covalent bonds, it is seen that SbOCl is more stable than $Sb_4O_5Cl_2$ and Sb_3O_4Cl; that is, $Sb(OH)Cl_2$ produced during the hydrolysis of $SbCl_3$ can continue on to eliminate HCl and generate SbOCl.

To further clarify whether the rupture and formation of covalent bonds during the hydrolysis of $SbCl_3$ is consistent with the results of the calculation, infrared spectroscopy was used to analyse the hydrolysis of $SbCl_3$ and the mechanism for formation of chlorine-oxygen covalent bonds.

3.2 Hydrolysis mechanism for antimony chloride systems

In the experiment, the filtrates from $SbCl_3$ hydrolysis, ethanolysis, and glycolysis were analysed by infrared spectroscopy [35-41] to determine the reaction pathway for $SbCl_3$ and the mechanism for replacement of chlorine by oxygen. The results are shown in Figure 3 and Figure 4. Characteristic infrared peaks are shown in Table 5.

Table 5. Infrared characteristic peaks

Key types	O-H	C-C	Alcohol C-O	$-CH_3$	$-CH_2-$
Absorption peak position（cm^{-1}）	3350~3200（Stretching） ~1595（Bending） 750~650（Out-of-plane bending）	400~900	1260~1000	~2870（Symmetric） ~2960（Asymmetric） ~1380（Symmetric deformation）	~2925（Asymmetric） ~2850（Symmetric） 1480~1440（Scissor）

3.2.1. Infrared spectroscopy of antimony oxychloride prepared by hydrolysis

Figure 3 shows the infrared spectrum of the hydrolysis product from solid $SbCl_3$. From A and B in Figure 3, it can be seen that the peak at 3313.21 cm^{-1} was due to the O-H stretching vibration, and the peak at 1634.38 cm^{-1} was due to the O-H intermolecular bending vibration. After adding $SbCl_3$, the hydrolysis of $SbCl_3$ facilitated the ionization of hydroxyl groups in water, the number of free hydroxyl groups in solution increased, and the concentration of hydroxyl groups was relatively increased. The H atom of [H-OH] formed an [Sb-OH] monomer. For [Sb-OH], there is a hydrogen bond between the oxygen atom of the -OH in the monomer and a water molecule that is not easy to break. The electronegativity of chlorine is 3.16, the electronegativity of hydrogen in water is 2.1, and free Cl ions are produced in water. It is easy to replace the hydrogen atom in the hydroxyl group to form [Cl-O-Sb], that is, SbOCl, since the Sb nucleus is larger than the H nucleus, and it is easy to form $Sb[OH]_3$ with the hydroxyl groups generated by ionisation of water. Because $Sb[OH]_3$ is unstable, it continued to hydrolyse to form SbOCl, Sb_3O_4Cl and $Sb_4O_5Cl_2$. Cl replaced the H atom in the water hydroxyl group so that the electron density increased, the force constant k increased, and an inductive effect was induced. The group frequency shifted to a higher wavenumber, the infrared spectrum of the water was redshift, and the electronegativity of the element increased. The stronger the inductive effect was, the more obvious the shift of the absorption peak to a higher wavenumber.

By comparing A and B in Figure 3, it can be seen that the absorption peak at 1634.38 cm^{-1} only shifted by 0.12 cm^{-1}, while the absorption peak at 3331.21 cm^{-1} shifted by 2.39 cm^{-1}; this clearly illustrates that the redshift of the absorption peak at 3313.21 cm^{-1} was not only due to the increased concentration of hydroxyl groups in solution but was also due to the inductive effect of the chlorine that replaced the hydrogen in the hydroxyl group.

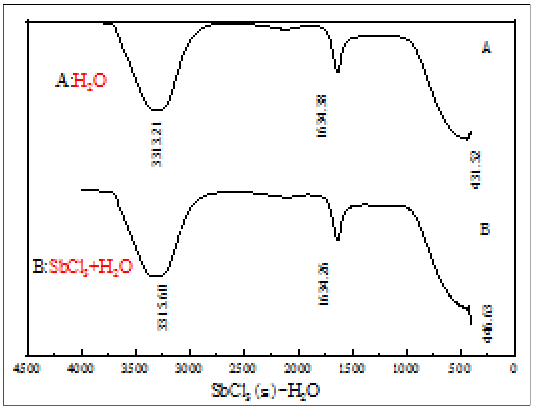

Figure 3. Infrared spectroscopy analysis of hydrolysis of $SbCl_3$ solid (A-H_2O B-$SbCl_3$+H_2O)

3.2.2. Infrared spectroscopy of antimony oxychloride prepared by alcoholysis in ethanol

Figure 4 shows the infrared spectrum for the alcoholysis of $SbCl_3$ solid in ethanol.

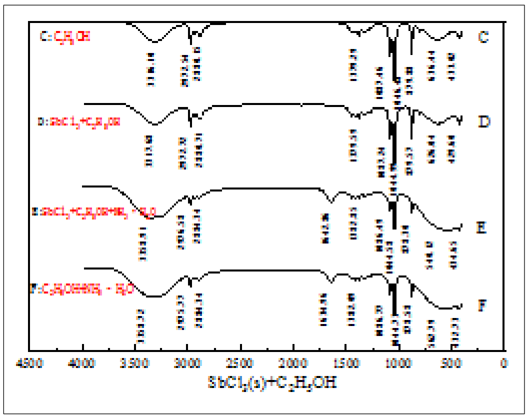

Figure 4. Infrared spectroscopy analysis of ethanol alcoholysis of solid $SbCl_3$
(C-C_2H_5OH, D-$SbCl_3$+C_2H_5OH, E-$SbCl_3$+C_2H_5OH+$NH_3 \cdot H_2O$, F-C_2H_5OH+$NH_3 \cdot H_2O$)

It can be seen from line C in Figure 4 that the absorption peak at 3316.10 cm^{-1} was caused by an OH stretching vibration, the absorption peak at 2972.54 cm^{-1} was caused by a -CH asymmetric contraction vibration in -CH_3, the peak at 2880.15 cm^{-1} was generated by the -CH symmetric contraction vibration in -CH_3, the peak at 1379.29 cm^{-1} was generated by the -CH symmetric deformation vibration in -CH_3, and the peak at 2880.15 cm^{-1} was generated by the symmetric stretch of -CH in -CH_2. The -CH in -CH_2 generated a peak at 1379.29 cm^{-1} due to shear vibration. The absorption peaks at 1087.46 cm^{-1} and 879.88 cm^{-1} were generated by C-C bond stretch vibrations. The peak at 1046.48 cm^{-1} was caused by a C-O stretching vibration, and the absorption peak at 636.44 cm^{-1} was caused by an -OH out-of-plane bending vibration.

From the comparison between the D and C spectra in Figure 4, it can be seen that the absorption peak at 3316.10 cm^{-1} shifted by 1.58 cm^{-1}, and the absorption peak at 636.44 cm^{-1} shifted by 10.4 cm^{-1} to low frequency. After the H on -OH was replaced by Cl, the electron cloud density increased and the force constant k increased as a result of the inductive effect; therefore, the band at 3316.10 cm^{-1} shifted to a higher wavenumber, and the infrared spectrum of ethanol redshifted. The electronegativity of Cl (3.16) is greater than that of H (2.1). After Cl replaced the H on -OH, a [C-O-Cl] monomer was formed. Since the electronegativity difference for the bonded atoms is greater, the absorption peak was stronger, the polarity was stronger, and the absorption peak was redshift; the weaker the polarity, the more the absorption peak was blueshift. Therefore, the polarity of -OCl is less than that of -OH, so the absorption peak at 636.44 cm^{-1} shifted to lower frequency and a blueshift occurred, which proves that the H on -OH was replaced by Cl.

Since the alcoholysis of SbCl$_3$ in ethanol was slow, the reaction was promoted by adding ammonia. By comparing lines E and F in Figure 4, we can see that the peak at 1634.96 cm^{-1} was caused by the stretching vibration of the -NH bond in -NH$_3$, and the absorption peak at 3358.72 cm^{-1} redshift by 0.19 cm^{-1} and at 562.79 cm^{-1} blueshift. by 22.67 cm^{-1}. That verifies the occurrence of an SbCl$_3$ substitution reaction in ethanol.

3.2.3. Infrared spectroscopy of antimony oxychloride prepared by glycolysis

To further clarify the mechanism of the SbCl$_3$ hydrolysis process, it was determined whether an alcoholysis reaction of SbCl$_3$ would occur in ethylene glycol. The results show that the absorption peak at 3329.97 cm^{-1} in line G line was caused by an -OH stretching vibration, the absorption peaks at 2936.68 cm^{-1} and 2873.77 cm^{-1} were caused by -CH$_2$ asymmetric and symmetric stretching, respectively, the 1408.20 cm^{-1} absorption peak was caused by a -CH$_2$ bending vibration, the peak at 1204.06 cm^{-1} was caused by a C-C stretching vibration, the peaks at 1082.99 cm^{-1} and 1031.95 cm^{-1} were caused by C-O bond stretching vibrations, the peaks at 881.27 cm^{-1} and 860.18 cm^{-1} were produced by two -OH out-of-plane bending vibrations; since the vibrational frequency of the two [CH$_2$OH] chemical bonds is the same, vibrational coupling occurred between them, causing the frequency of one of the peaks to be higher than the original frequency and the frequency of the other peak to be lower.

From a comparison of the H and G spectra in Figure 5, it can be seen that the band at 3329.97 cm^{-1} exhibited a shift of 9.99 cm^{-1} to lower frequency. This is because the electronegativity of Cl (3.16) is greater than that of H (2.1), and Cl replaces -OH. After H loss, the formation of the [C-O-Cl] monomer occurred; the absorption peak at 881.27 cm^{-1} was redshift by 0.19 cm$^{-1,}$ and the absorption peak at 860.18 cm^{-1} was blueshift by 0.01 cm^{-1}. One of the -OH groups in the alcohol was replaced by Cl, and the other was not, resulting in an increase in the electron density of the substituted -OH, an increase in the force constant k, and an inductive effect causing the absorption at 881.27 cm^{-1} to redshift, while the absorption peak at 860.18 cm^{-1} was blueshift.

The alcoholysis reaction of solid SbCl$_3$ was slow in ethylene glycol, so the reaction was promoted by adding ammonia water. By comparing lines I and J in Figure 5, it can be seen that the peak at 1643.32 cm^{-1} was caused by the stretching vibration of the -NH bond in NH$_3$. There are absorption peaks at 3284.52 cm^{-1}, 882.33 cm^{-1} and 860.99 cm^{-1} and the absorption peak at 3284.52 cm^{-1} was blueshift by 4.88 cm^{-1}, the peak at 882.33 cm^{-1} was blueshift by 0.33 cm^{-1}, and the peak at 860.99 cm^{-1} was redshift by 0.33 cm^{-1}, further verifying that the substitution of SbCl$_3$ occurred in ethylene glycol.

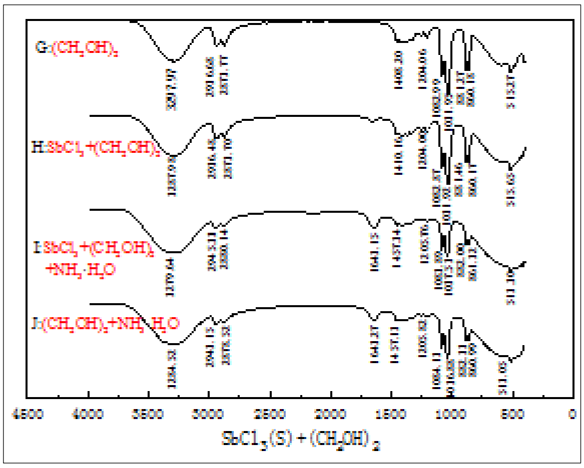

Figure 5. Infrared spectroscopy analysis of glycol alcoholysis of $SbCl_3$ solid. (G-$(CH_2OH)_2$ H-$SbCl_3+(CH_2OH)_2$ I-$SbCl_3+(CH_2OH)_2+NH_3·H_2O$ J-$(CH_2OH)_2+NH_3·H_2O$)

3.2.4. Hydrolysis mechanism of antimony in the Sb^{3+}-HCl system

To verify whether the hydrolysis, alcoholysis, and glycolysis of solid $SbCl_3$ were consistent with the Sb^{3+} hydrolysis process occurring in aqueous solution, $SbCl_3$ solutions with concentrations of 0.05 mol/L Sb^{3+} and 1 mol/L Cl^- were prepared for studies of hydrolysis and alcoholysis. The reactions were carried out under the same conditions, and the products were analysed by infrared spectroscopy. The results are shown in Figure 6. By comparison, it was found that the infrared spectrum was completely consistent with that from the reaction of solid $SbCl_3$, which confirms the mechanism of the $SbCl_3$ hydrolysis process. There are two main ways to hydrolyse $SbCl_3$ into oxychloride: 1) water and alcohol ionise hydroxyl groups and replace a Cl atom in $SbCl_3$ to form $[Sb(OH)Cl_2]$ monomer; as the degree of hydrolysis progresses, the monomer loses H and Cl to form SbOCl, Sb_3O_4Cl, and $Sb_4O_5Cl_2$; 2) Sb directly forms [Sb-OH] monomer with OH ionised by water and alcohol, and Cl replaces the H on the [Sb-OH] hydroxyl group in the monomer and directly forms SbOCl, Sb_3O_4Cl, and $Sb_4O_5Cl_2$.

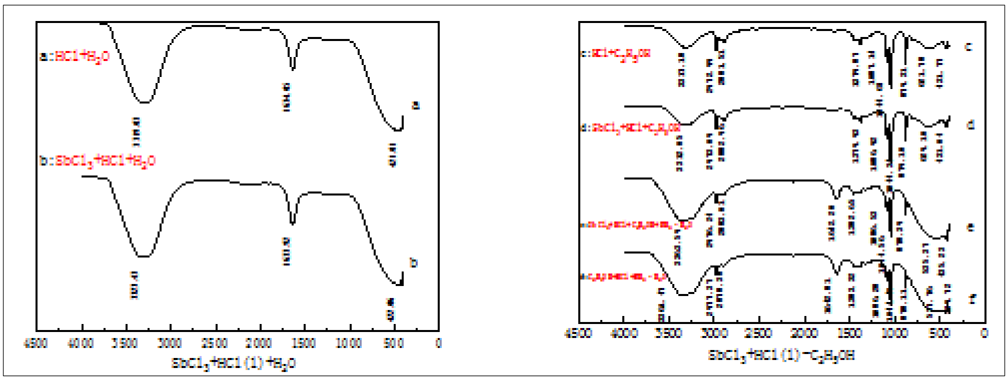

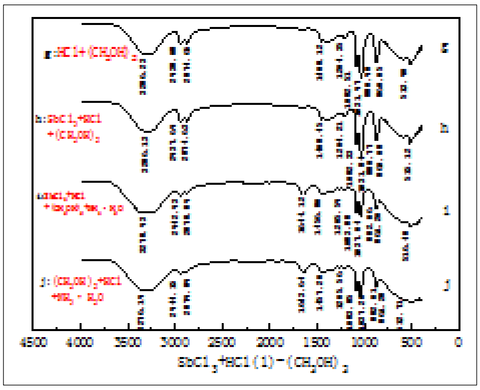

Figure 6. Infrared spectroscopy analysis of $SbCl_3$ and HCl of hydrolysis, ethanol alcoholysis and glycol alcoholysis reaction. (a-$HCl+H_2O$, b-$SbCl_3+HCl+H_2O$, c-$HCl+C_2H_5OH$, d-$SbCl_3+HCl+C_2H_5OH$, e-$SbCl_3+HCl+C_2H_5OH+NH_3·H_2O$, f-$C_2H_5OH+HCl+NH_3·H_2O$, g-$HCl+(CH_2OH)_2$, h-$SbCl_3+HCl+(CH_2OH)_2$, i-$SbCl_3+HCl+(CH_2OH)_2+NH_3·H_2O$, j-$(CH_2OH)_2+HCl+NH_3·H_2O$)

4. Conclusions

(1) The density functional method was used to calculate the electronic properties of $SbCl_3$, SbOCl, Sb_3O_4Cl, and $Sb_4O_5Cl_2$ unit cells using analyses of unit cell structure, unit cell energy, energy band, total density of states, partial density of states, overlap populations, formal charges, and covalent bond properties of $SbCl_3$, SbOCl, Sb_3O_4Cl, and $Sb_4O_5Cl_2$ in their respective unit cells. This was combined with information from analysis of infrared spectroscopic data for hydrolysis reactions leading to antimony oxychloride by atom transfer. There are two main ways to hydrolyse $SbCl_3$ into oxychloride: the hydroxyl groups in water and alcohol are ionised to replace one Cl atom in $SbCl_3$ and form a $[Sb(OH)Cl_2]$ monomer. During further hydrolysis, H and Cl atoms are removed. Alternatively, SbOCl, Sb_3O_4Cl, and $Sb_4O_5Cl_2$ or Sb atoms are formed directly from [Sb-OH] monomers with OH ionised by water or alcohol. Cl atoms replace the H atoms on the hydroxyl groups in [Sb-OH] monomers to form SbOCl, Sb_3O_4Cl, and $Sb_4O_5Cl_2$ directly.

(2) Infrared spectroscopy indicated that with $SbCl_3$ in the water, ethanol, and ethylene glycol systems, the water hydroxyl group and alcohol hydroxyl group exhibited redshift and blueshift in the infrared spectra; the hydroxyl band at high frequency changed because the chlorine atom replaced the hydrogen atom, and the electron density increased. The force constant k increased, an inductive effect occurred, the group frequency shifted to higher wavenumber, the infrared spectrum was redshift; since the polarity of the -OCl bond is weaker than that of the -OH bond, the hydroxyl vibration shifted to lower frequency. A blueshift occurred, which indicates that the hydrogen atom on -OH was replaced by a chlorine atom; this is consistent with the calculated results on the strength of the covalent bond between chlorine and oxygen, which confirms the results of the density functional method.

Acknowledgements: This paper has been financially supported by the National Natural Science Foundation of China (No.U1802251), Jiangxi Provincial Department of Science and Technology Project(NO.20212AEI91003),Jiangxi Provincial Department of Education Science and Technology Project (No. GJJ180466).Special thanks also go to staff at Jiangxi Copper Corporation Limited Guixi Smelter for providing the Copper anode slime materials used in this study.

References

1.YANG H-Y, LI X-J, TONG L-L, et al., Process mineralogy of high lead copper anode slime [J]. The Chinese Journal of Nonferrous Metals, 2014, 24(01): 269-278.
2.WANG X-W, CHEN Q-Y, YIN Z-L, et al., Identification of arsenato antimonates in copper anode slimes[J]. Hydrometallurgy, 2006, 84(3-4): 211-217.
3.ZHONG S-P, WANG J, ZHANG H-R, et al., Extraction Technology of Copper Anode Slime by Caldo Furnace Method[M], 2019(Metallurgical Industry Press).
4.HOU H-F., Complex Recovery ofNon-ferrous, Rare and Noble Metals from Copper Anode Slime [J]. SHANGHAI NONFERROUS METALS, 2000(02): 88-93.
5.KONG X-F, DENG J-H., Research Status of Copper Anode Sludge Treatment [J]. World Nonferrous Metals, 2019(19): 169+171.
6.ZHANG B-Y, WANG J-K., Production practice of copper anode slime treatment by dressing-metallurgy combination method[J]. China Nonferrous Metallurgy, 2007(03): 59-62.
7.JIN Z-N，MA Z-Y，YANG H-Y, et al., Behaviors of Precious and Base Metals in Process of Copper Anode Slime Hydrometallurgical Treatment [J]. Journal of Northeastern University(Natural Science), 2015, 36(09): 1305-1309.
8.YE L-G, ZHEN O-Y, CHEN Y-M, et al., Selective separation of antimony from a Sb-Fe mixed solution by hydrolysis and application in the hydrometallurgical process of antimony extraction[J]. Separation and Purification Technology, 2019:115753.
9.ZHENG Y-J, TENG H, BAI M., Preparation of high-purity antimony oxychloride from high-arsenic refined bismuth dust[J]. Journal of Central South University：Science and Technology, 2011,(6)：1549-1554.

10.ZHANG D-M, XIAO S-W., Ostwald rule and the polymorphous control of antimony white prepared by wet method[J]. Journal of Central South University of Technology(Natural Science), 2000,(2):121-123.
11.LING M, ZHANG S-G, PAN D.-A., et al., Antimony recovery from $SbCl_5$ acid solution by hydrolysis and aging[J]. Rare Metals, 2015,34(06):436-439.
12.ZHENG G-Q., ZHI B., CHEN J-Z., Hydrolysis of antimony pentachloride[J], The Chinese Journal of Nonferrous Metals, 2006, (9):1628-1633.
13.A. KOLIADIMA, A. HENGLEIN, E. MATIJEVIC. Colloidal hydrolysis products of $SbCl_3$ in acidic solutions[J]. Colloid and Polymer Science, 1997, Vol.275(NO.10):972-978.
14.A.E. PANASENKO, L. A. ZEMUKHOVA, L. N. IGNATEVA, et al., Phase composition of antimony(III) oxide samples of different origin[J]. Inorganic Materials, 2009, Vol.45(No.4):402-408.
15.U. YUCELIK ÖZER, R. F. BOGUCKI. Equilibrium studies of antimony(III) chelates in aqueous solution[J].Journal of Inorganic and Nuclear Chemistry, 1971,Vol.33(No.12):4143-4153.
16.NEELAM YADAV, MEENA NAGER, RAKESH BOHRA, New sol–gel precursors for binary oxides of antimony, Sb_2O_3 (senarmonite) and α-Sb_2O_4: synthesis and characterization of some ketoximate modified antimony(III) alkoxides[J].Journal of Sol-Gel Science and Technology, 2010, Vol.54(No.1):119-128.
17.TIAN Q-H., XIN Y-T.Y., YANG L., et al. Theoretical simulation and experimental study of hydrolysis separation of $SbCl_3$ in complexation-precipitation system[J]. Transactions of Nonferrous Metals Society of China, 2016, 26(10):2746-2753.
18.DU X-L. Research on the hydrolysis equilibrium of antimony trichloride in the Sb^{3+}-Cl^--H_2O system[J]. China Nonferrous Metallurgy, 2012, (5).
19.ZHENG G-Q, HUANG R-B, PAN Y, et al., Phases of antimony trichloride solution containing fluorine neutralization-hydrolysis products[J]. The Chinese Journal of Nonferrous Metals, 2005, 15(8): 1278-1282.
20.CLARK S J., SEGALLII M D., PICKARDII C J., et al., First principles methods using CASTEP[J]. Zeitschrift für Kristallographie, 2005, 220(5-6).
21.MILMAN V., REFSON K., CLARK S J., et al., Electron and vibrational spectroscopies using DFT, plane waves and pseudopotentials: CASTEP implementation[J]. Journal of Molecular Structure THEOCHEM, 2010, 954(1):22-35.
22.NI Z , GUO X , LIU X., et al., Understanding the magnetic structural transition in all-d-metal Heusler alloy $Mn_2Ni_{1.25}Co_{0.25}Ti_{0.5}$[J]. Journal of Alloys and Compounds, 2019, 775:427-434.
23.FRANCISCO C , FERNANDEZ ANA MARIA, TIMON VICENTE, et al., Becquerelite mineral phase: crystal structure and thermodynamic and mechanical stability by using periodic DFT[J]. RSC Advances, 2018, 8(43):24599-24616.
24.DENG Y., EAMES C., NGUYEN L H B., et al., Crystal structures, local atomic environments and ion diffusion mechanisms of scandium-substituted NASICON solid electrolytes[J]. Chemistry of Materials, 2018:acs.chemmater.7b05237.
25.XIAO X., XING C., HE G., et al., Solvothermal synthesis of novel hierarchical Bi4O5I2 nanoflakes with highly visible light photocatalytic performance for the degradation of 4-tert-butylphenol[J]. Applied Catalysis B: Environmental, 2014, 148-149:154-163.
26.YUAN S, SUN Z, REN W, et al., First principles study of the magnetic properties and charge transfer of Ni-doped $BiFeO_3$[J]. Journal of Magnetism & Magnetic Materials, 2017, 449:S0304885317307461.
27.ZHANG S Y, HU C L, LI P X, et al., Syntheses, crystal structures and properties of new lead(II) or bismuth(III) selenites and tellurite[J]. Dalton Transactions, 2012, 41(31):9532-9542.
28.JIANG H Y., LI P., LIU G., et al., Synthesis and photocatalytic properties of metastable β-Bi_2O_3 stabilized by surface-coordination effects[J]. Journal of Materials Chemistry A, 2015, 3.
29.WU C., LU P., YU Z., et al., Structural and Electronic Properties of Neutral Clusters Al12X (X = P, As, Sb, and Bi) and Their Cations[J]. Journal of Computational and Theoretical Nanoscience, 2013, 10(5):1055-1060.

30.ZHANG X.-Y., ZHENG B.-J., GUO B., et al., First Principles Study on Electronic Structure and Corrosion Resistance of Fe-N-Cr[J]. Materials Reports, 2016, 30(18):155-158.
31.WANG M.-J., LI C.-F., WEN P., et al., The bond characters and phase stability effects of Cr Mo and Ni in bulk -Fe(C)[J]. Acta Physica Sinica, 2016, 65(3):246-255.
32.ZHANG P., ZHAO Q.-C., LIU J.-J., et al., Research on inhibitors and hindered groups in ultra-deep hydrodesulfurization based on density functional theory[J]. Catalysis Today, 2018:170-178.
33.XUE J.-X., ZHANG R.-G., LIU Y.-P., et al., The alloying of Ti, C, N in bulk α-Fe and their effects on bond characters[J]. Acta Physica Sinica, 2012, (12):427-434.
34.WEN P., LI C.-F., ZHAO Y., et al., First principles calculation of occupancy, bonding characteristics and alloying effect of Cr, Mo, Ni in bulk α-Fe(C) [J]. Acta Physica Sinica, 2014, (19):288-295.
35.YANG J.-M., ZHANG H.-M., WANG XU, et al., The Relationships and Differences Between the Infrared Spectrometry and Raman Spectrometry[J]. Physics and Engineering, 2014, 24(4):26-29.
36.WANG J.-Z., WANG T., How to Interpret Infrared (IR) Spectra[J]. University Chemistry, 2016, 31(6):90-97. DOI:10.3866/PKU.DXHX201504001.
37.HU H.-L., Raman Spectroscopy Analysis and Concentration Correlation Study of Ethanol-Water Solution[D]. Jiangsu: Nanjing University of Science and Technology 2012. DOI:10.7666/d.y2062091.
38.YUAN B., DOU X.-M., Near-Infrared Spectral Studies of Hydrogen-Bond in Water-Methanol Mixtures[J]. Spectroscopy and Spectral Analysis, 2004, 24(11):1319-1322.
DOI:10.3321/j.issn:1000-0593.2004.11.011.
39.XIE Y., YI J., ZHANG S., et al., Study on Ternary Mixtures of Water, Acetic Acid and Ethanol by Near Infrared Spectroscopy[J]. Chinese Journal of Spectroscopy Laboratory, 2003, 20(5):643-646.
DOI:10.3969/j.issn.1004-8138.2003.05.002.
40.ZHU C.-G., WANG F.-W., XU M., et al., Synthesis of Metal Alkoxide Complex and Nano-$NiFe_2O_4$ in $HOCH_2CH_2OH$ Solution[J]. Chinese Journal of Inorganic Chemistry, 2009, 25(7):1177-1181.
DOI:10.3321/j.issn:1001-4861.2009.07.007.
41.NEELAM YADAV, MEENA NAGAR, RAKESH BOHRA, New sol-gel precursors for binary oxides of antimony, Sb_2O_3 (senarmonite) and α-Sb_2O_4: synthesis and characterization of some ketoximate modified antimony(III) alkoxides[J].Journal of Sol-Gel Science and Technology, 2010, Vol.54(No.1):119-128.

Manuscript received: 8.07.2021